Improving the Performance of High-Density Platooning Using Vehicle Sensor-Based Doppler-Compensation Algorithms

Roman Alieiev, Guillaume Jornod, Thorsten Hehn, Andreas Kwoczek, and Thomas Kürner

***Abstract*— This paper investigates the advantages of using communication supported by information from vehicle sensors to improve the performance of the High-Density Platooning (HDPL) application. HDPL is one of the most promising applications in the field of cooperative driving. The goal of this application is to improve fuel and road efficiency without impairing safety. The level of efficiency improvement depends on the instantaneous channel quality. Strong multipath components, which arise from other vehicles, traffic signs, and surrounding buildings in such a highly dynamic vehicular environment, significantly influence the instantaneous link quality between communicating vehicles in a platoon. An emerging concept of vehicle sensor-aided predictive communications has shown its potential to improve direct-link communication. In this paper, the applicability of this approach is evaluated in terms of inter-vehicle distance error, which reflects the difficulties that the control algorithm has to cope with in the communications conditions. The simulation results show that the proposed sensor-based approach significantly improves the platoon performance even if affected by multiple dynamic scattering reflections at the same time.**

***Index Terms*— Channel modeling, high-density platooning, vehicle control, inter-vehicle communications, Doppler effect, fuel and road efficiency.**

I. Introduction

PLATOONING is one of the most promising services in cooperative vehicle automation. Cooperation among trucks in platoon allows for smaller headways between vehicles while assuring strict safety requirements [1]. The platoon with even further decreased headways distances is known as High-Density Platooning (HDPL). The main goals of HDPL are additional safety, increased road occupation efficiency and reduction of fuel consumption. The first two goals can be achieved by having a better coordination between road users [2] while aiming for headways below ten meters. Reduction of fuel consumption arises from multiple factors, for instance from the mitigated accordion effect or reduced drag force in shortened inter-vehicle distances (IVDs) [3]. Hence, finding the ways to improve cooperation efficiency among vehicles is currently one of the most researched topics in the field of cooperative vehicle automation [4], [5] in general and HDPL [6] in particular.

The major motivation to study the applicability of new communication methods for HDPL is that the cooperation efficiency among vehicles in HDPL strongly relies on the quality of the vehicle-to-vehicle (V2V) communication link [7].

Enabling effective and stable V2V communication link in a highly dynamic environment brings many unresolved challenges [8]. From the V2V signal propagation prospective, examples include: considerably large relative speeds with respect to other road participants; highly non-uniform angular distribution of received energy due to closely located scattering objects (*e.g.*, houses, road infrastructure or other vehicles with flat surfaces and large reflectivity coefficients); antenna heights comparable to scatterers' heights, *etc*.

Moreover, multiple measurement campaigns [9]–[11] confirm that the observed Doppler frequency shift as a function of time coincides with the presence of scatterers along the driven path. As a result, significant frequency shifts may affect both the directly propagated line-of-sight (LOS) and the reflected signal components. Depending on the relative traveling direction, the Doppler shift of the signal reflected from other vehicles on the road may increase by a factor of four, resulting in dramatic impact onto the received signal. At the same time, if the reflected signal is not affected by the frequency shift or if the Doppler can be compensated, it can bring additional gain to the communication link. In other words, the same reflecting object on the road can bring positive or negative contributions to the communication process depending on its relative position, dynamics and the ability of communications system to adapt to time-varying channel conditions. Such highly challenging channel results in instabilities on the link-level performance, which in turn impacts the performance of cooperative driving applications, including HDPL.

These challenges can be reduced if an information about the dynamic surrounding environment is provided as an additional information to the V2V communications system. A novel approach of sensor-aided Doppler-shift compensation [12], [13], which benefits from vehicle sensor data, has shown high potential to improve V2V link level performance. The concept links information about the dynamic road environment generated by vehicle sensors for automated driving

Manuscript received November 27, 2017; revised June 30, 2018 and December 23, 2018; accepted March 11, 2019. Date of publication April 26, 2019; date of current version December 31, 2019. The Associate Editor for this paper was X. Cheng. *(Corresponding author: Roman Alieiev.)*

R. Alieiev is with MAN Truck and Bus, 80995 Munich, Germany, and also with the Technische Universität Braunschweig, 38106 Braunschweig, Germany (e-mail: roman.alieiev@man.eu).

G. Jornod is with Volkswagen Group, 38436 Wolfsburg, Germany, and also with the Technische Universität Braunschweig, 38106 Braunschweig, Germany (e-mail: guillaume.jornod@volkswagen.de).

T. Hehn is with Audi AG, 85057 Ingolstadt, Germany (e-mail: thorsten.hehn@audi.de).

A. Kwoczek is with Volkswagen Group, 38436 Wolfsburg, Germany (e-mail: andreas.kwoczek@volkswagen.de).

T. Kürner is with the Technische Universität Braunschweig, 38106 Braunschweig, Germany (e-mail: kuerner@ifn.ing.tu-bs.de).

Digital Object Identifier 10.1109/TITS.2019.2909569

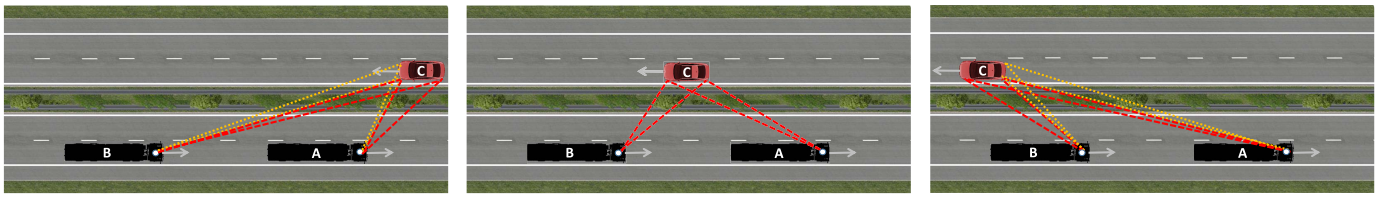

(a) (b) (c)

Fig. 1. An illustrative scenario: a platoon and a light passenger car passing each other, depicted in three different time instances. Depending on a relative position, either one or two sides (depicted in yellow and red colors) of a scattering vehicle contribute to strong reflection.

maneuver tasks with a communications system. One of its direct advantages is an ability to track main road objects and to derive expected Doppler properties from them. This allows minimizing the negative impact from some of the most challenging channel components with high Doppler shift.

The goal of this paper is to show that the use of information about surrounding environment provided by vehicle sensors can also improve the performance of the HDPL application. We hope that this analysis will bring more attention into the use of vehicle sensor data for the tasks of improving stability of cooperative vehicular applications, such as HDPL.

In particular we investigate the following challenges and bring the following key contributions:

1) the paper highlights the challenges of HDPL which arise from surrounding scattering objects in terms of link-level parameters and elaborates the subsequent application-level changes, *i.e.*, target IVD, acceleration, velocity, and their impact on the driving comfort level and fuel consumption.
2) the paper motivates and shows the benefit of using the sensor-based Doppler-shift compensation for the HDPL application in highly dynamic vehicular environment.

The paper is organized as follows: Section II introduces the problem of Doppler frequency shift in HDPL and shows how the use of sensor-based predictive communications could minimize this problem; Section III describes the implementation flow of the HDPL application used in this paper; Section IV presents the simulation setup of the scenario of interest and evaluates the obtained results. Section V concludes the paper.

II. Sensor-Based Doppler-Compensation for High-Density Platooning

In this section, we first introduce the problem of Doppler frequency shift in the scope of HDPL. We then present our system model and the applied sensor-based channel prediction method.

A. The Problem of Doppler Frequency Shift in HDPL

One of the most straightforward and widely studied scenarios in which Doppler frequency shift impacts V2V communications performance is when cooperating cars drive in opposite directions (OD). First, cars are characterized by the highest velocities among road participants. Second, due to opposite driving directions, the relative velocity between two cars may reach the double of the single car velocity, resulting in very challenging Doppler impact.

Nevertheless, there exists less obvious and subsequently less studied other essential and challenging scenarios where the presence of Doppler-frequency shift may significantly impact the performance of the vehicle driving maneuvers. HDPL affected by strong single-bounce reflections belongs to such scenarios.

In contrast to the OD scenario, Doppler shifts affecting communications among HDPL originate from the reflected signal components and not from the relative velocity between communicating partners. Fig. 1 illustrates an example of this scenario, in which a passenger vehicle passes a truck platoon. Although the frequency shift of the LOS component between two vehicles in the platoon is low, the Doppler shift from the single bounce reflection can be high, time-varying and, in some situations, can reach frequency shifts arising from the combined absolute velocities of communicating vehicles plus the doubled velocity of a scattering vehicle. Fig. 2 highlights simulation examples of possible Doppler shifts (a) and received reflected power (b) for three typical scenarios, *viz.* "light vehicle passes truck platoon on the highway", "truck passes the truck platoon on the highway" and "light vehicle passes the truck platoon on the rural road". Here, in all scenarios, the road situation is similar to the one presented in Fig. 1. In the highway scenario, the lanes between the platoon and a passing-by vehicle are separated by 13 m, whereas in the rural scenarios, the separation distance is only 3 m. The results of the two scenarios are shown for both 5 and 14 m platoon headways distance. Both the Doppler shift and the received signal power are time- and space-variant in the environment with highly dynamic communication partners. Moreover, the highest impact of Doppler frequency shift can be observed in the regions from 10 m to 0 m (approaching each other) and from -30 m to -40 m (moving away from each other). In this region both the power and Doppler shift of the received signal are near their maxima.

B. System Model

To highlight the nature of the problem, let us consider two vehicles involved in a cooperative HDPL maneuver. At the application level, the cooperative adaptive cruise control (CACC) function periodically generates a control message, which is then being sent to the other platoon vehicles. Depending on the channel conditions, some transmitted messages may be lost at the receiver and the HDPL function at the receiving truck has to rely on its local sensors only,

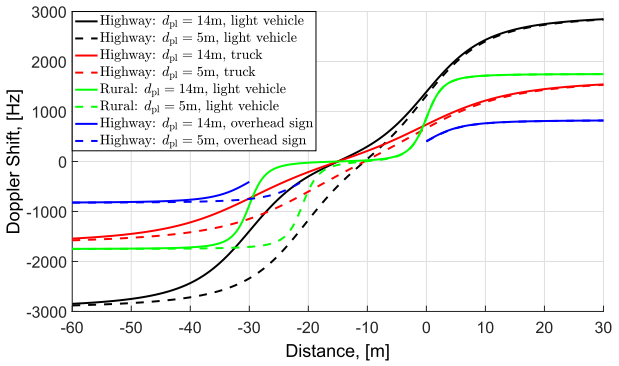

(a)

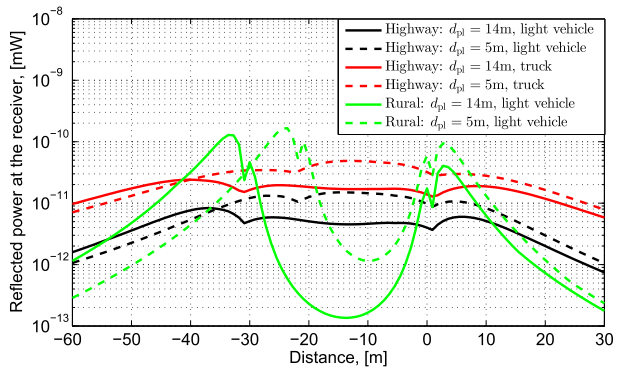

(b)

Fig. 2. The impact of the single bounce reflection on HDPL over distance between the first communication vehicle and the reflecting object projected on the HDPL traveling direction for different road scenarios (highway and rural), distances between vehicles in the platoon d_{pl} and a type of vehicles in the platoon. Possible levels of Doppler-shift for the reflected component are shown above (a), simulated reflected powers at 5.9GHz carrier frequency are shown below (b).

resulting in a temporary switch from CACC to adaptive cruise control (ACC).

At the link level, we assume Long-Term Evolution (LTE)-Sidelink with single-carrier frequency-division multiple access (SC-FDMA)-based frame structure, which is a basis for the V2V applications over LTE [14]. In such a system, the pilot symbols for channel estimation are located at the fourth and eleventh orthogonal frequency-division multiplexing (OFDM) symbols spanning the entire scheduled subcarrier range. Then, the received sample $y[k, \tau]$ at the sampling time $[k]$, affected by the propagation delay τ, has the following form:

$$y[k] = h[k, \tau] * x[k] + n[k], \tag{1}$$

where, $x[k]$ is the transmitted sample, $n[k]$ is additive white Gaussian noise and $h[k, \tau]$ is the time-varying channel impulse response (CIR), defined as:

$$h[k, \tau] = h_{\mathrm{LOS}}[k, \tau] + \sum_{s=1}^{S} h_{\mathrm{Rs},s}[k, \tau] + h_{\mathrm{Dif}}[k, \tau], \tag{2}$$

where $h_{\mathrm{LOS}}[k, \tau]$ is LOS component and $h_{\mathrm{Rs},s}[k, \tau]$ is the sth reflection from a mobile or static object, resolved at the receiver; $h_{\mathrm{Dif}}[k]$ represents all remaining non-resolved and diffuse components.

From the LTE-Sidelink perspective, the received resource element at the ith symbol and jth subcarrier is obtained via the Fourier transformation from the multiple time-domain samples, each of which is affected by the channel as described in Eq. (2). This results in the following representation in the subcarrier-symbol grid (denoted by the sc-term):

$$y^{\mathrm{sc}}_{i,j} = h^{\mathrm{sc}}_{i,j} x^{\mathrm{sc}}_{i,j} + r^{\mathrm{sc}}_{\mathrm{ICI}_{i,j}} + n^{\mathrm{sc}}_{i,j}, \tag{3}$$

where $h^{\mathrm{sc}}_{i,j}$ is the channel, $x^{\mathrm{sc}}_{i,j}$ is the resource element transmitted at subcarrier-symbol position i, j, corrupted by the inter-carrier interference (ICI) $r^{\mathrm{sc}}_{\mathrm{ICI}_{i,j}}$ and the additive white Gaussian noise $n^{\mathrm{sc}}_{i,j}$. As we can see from Eq. (2) and Eq. (3), every received resource element $y^{\mathrm{sc}}_{i,j}$ component is dependent from the physical properties of the surrounding objects.

Finally, besides the ICI σ^2_{ICI} and noise σ^2_N power, the performance of HDPL will also depend on the ability of the communications system to obtain channel coefficients at data positions from the estimated channel at the pilot positions. This results in the following mean square error (MSE) [15]:

$$\sigma^2_e = \mathbb{E}\left\{\|h^{\mathrm{sc}}_{i,j} - \hat{h}^{\mathrm{sc}}_{i,j}\|^2\right\} = c_e(D)(\sigma^2_N + \sigma^2_{\mathrm{ICI}}) + d(D, f_{\mathrm{D}}), \tag{4}$$

where $\hat{h}^{\mathrm{sc}}_{i,j}$ is the estimated channel, $d(D, f_{\mathrm{D}})$ is the additional error at data resource elements and $c_e(D)$ is a scalar, which depends on the pilot symbols pattern defined by D [15].

Existing approaches usually find channel coefficients at data positions by interpolating the pilot estimates or by exploiting the channel statistics. Both approaches result in significant estimation error for non-stationary and time variant channels, which are common in vehicular communications. In this paper, we minimize this error by applying a sensor-based channel prediction and Doppler compensation method, which has shown its suitability for highly dynamic vehicular channels [12].

C. Sensor-Based Channel Prediction for HDPL

Scatterers which are located along the road have deterministic properties, such as lateral and longitudinal locations, heights, densities, dimensions, dynamics, *etc*. Resulting from the functional requirements for automated driving maneuvers in modern vehicles, many of these road objects and their properties can be detected and tracked by complex on-board sensor systems [16], [17]. This enables an application of context-aware methods as an additional independent information source to improve communication algorithms [18], [19]. The vehicle sensor-aided predictive communication introduced by the same authors in [12], and further elaborated in [13], [20], [21], is one of the promising methods which utilizes context awareness to improve wireless communications. Compared to other methods, which mainly address cellular based communications [22], [23] or apply channel prediction without the use of sensor data [24], this approach is specifically designed to utilize vehicle sensor data for direct-link V2V communications. Such vehicle sensor-based prediction allows to minimize the negative impact of some signal components at the expected time. In the present work, we investigate the

applicability of this approach to improve the performance of the HDPL application. For this, we restrict our attention to the impact of strong single-bounce reflections from surrounding objects on key performance indicators of truck platooning and investigate the resulting potential application gain and limitations from it.

According to [12], the vehicle sensor-aided communications system enables prediction of dynamic V2V communication link parameters, such as the expected Doppler shift of the dominant channel component, which is conducted in the following steps:

1) **obtain** sufficient knowledge about absolute properties, such as absolute position, velocity, and corresponding relative changes with respect to other detected objects in the surrounding environment;
2) **extract** information from environmental knowledge;
3) **conduct** prediction based on the available information;
4) **reconfigure** communications system properly and in timely manner;
5) **control** the prediction quality via a feedback loop.

For the case of HDPL, these steps represent a complex set of relationships between different functional components within a group of communicating vehicles on the road. The environmental perception unit utilizes onboard sensor data combined with the data provided by other vehicles in the vicinity, *e.g.* via collective perception [25], [26]. At the next step, the scene understanding and object classification is conducted by the available algorithm used by the maneuver planning tasks. Since the onboard maneuver planning function inherently requires real-time performance capabilities, this makes the model be suitable for the sensor-based prediction tasks as well.

Each detected object represents an oversimplified cuboid bounded by six quadrilateral faces. The velocity and coordinates of the geometrical center of each face is then provided as a reference point to the prediction algorithm. This approach allows each communicating partner to obtain information about the position and the planned trajectory of other vehicles in its vicinity. If the vehicle equipped with sensors is capable of detecting surrounding objects, then information about large scattering objects (their dimensions, absolute and relative positions) is also used for communications prediction.

We restrict our scope to the scenario presented in Fig. 1 extended to three platooning vehicles and multiple oncoming vehicles causing dynamic scattering reflections. Moreover, we consider the simplest set of available sensors providing information about the absolute velocity and the planned trajectory (heading) of vehicles in the vicinity. The accuracy of such a model is limited by two factors: the vehicle sensor accuracy and the mismatch between the reference point and the actual region with the strongest reflection. This mismatch is caused by simplification assumptions in the current modeling: the detected scattering objects are assumed to have flat surfaces with strongest reflection in the middle of the reflecting side, whereas in reality, it depends on the shape, relative position and relative angle of the scattering object. This results in a time-varying precision mismatch ranging from tens of centimeters (only sensor inaccuracy) up to few meters (sensor inaccuracy and reference point mismatch).

At the next step, the strongest reflecting object is selected among all detected deterministic objects (the selection is based on the function which compares all products of the path loss and the scattering cross-section for each detected scattering object). Then, we calculate the projections of the estimated velocities vectors onto the LOS direction for communicating vehicles and onto directions between each communicating vehicle and the scattering objects of interest.

According to Fig. 1, the communicating vehicles are denoted by "A" and "B", the dominant scattering vehicle by "C". Then the line segments between them will be "AB", "AC", "BC". The angles between the heading directions (unit vectors) of each vehicle, *i.e.* $\vec{\mathrm{A}}$, $\vec{\mathrm{B}}$, $\vec{\mathrm{C}}$, and the corresponding line segments are $\theta_{\vec{\mathrm{A}},\mathrm{AC}}$, $\theta_{\vec{\mathrm{A}},\mathrm{AB}}$, $\theta_{\vec{\mathrm{B}},\mathrm{BC}}$, $\theta_{\vec{\mathrm{B}},\mathrm{AB}}$, $\theta_{\vec{\mathrm{C}},\mathrm{AC}}$, $\theta_{\vec{\mathrm{C}},\mathrm{BC}}$.

Projecting the estimated velocities vectors of communicating vehicles onto "AB" (the LOS direction) and the scattering vehicle "C" onto "AC' and "BC" (the directions of the dominant scattering components), the Doppler frequency shift of the LOS $\tilde{f}_{\mathrm{D_{LOS}}}$ and the dominant reflection component $\tilde{f}_{\mathrm{D_C}}$ can be found as:

$$\begin{cases} \tilde{f}_{\mathrm{D_{LOS}}} = \dfrac{f_\mathrm{c} \cdot (\mathrm{Pr}_{\vec{\mathrm{A}}}\mathrm{AB} \cdot \tilde{v}_\mathrm{A} + \mathrm{Pr}_{\vec{\mathrm{B}}}\mathrm{AB} \cdot \tilde{v}_\mathrm{B})}{c}, \\ \tilde{f}_{\mathrm{D_C}} = \dfrac{f_\mathrm{c} \cdot (\mathrm{Pr}_{\vec{\mathrm{A}}}\mathrm{AC} \cdot \tilde{v}_\mathrm{A} + \tilde{v}_\mathrm{C}(\mathrm{Pr}_{\vec{\mathrm{C}}}\mathrm{AC} + \mathrm{Pr}_{\vec{\mathrm{C}}}\mathrm{BC}) + \mathrm{Pr}_{\vec{\mathrm{B}}}\mathrm{BC} \cdot \tilde{v}_\mathrm{B})}{c}, \end{cases} \tag{5}$$

where $\tilde{v}_\mathrm{A}$, $\tilde{v}_\mathrm{B}$, $\tilde{v}_\mathrm{C}$ are the absolute values of the estimated velocities of vehicles "A", "B" and "C", respectively; f_c is the carrier frequency and c is the speed of light; $\mathrm{Pr}_{\vec{\mathrm{X}}}\mathrm{XY} \cdot \tilde{v}_\mathrm{X}$ is the projection operation of a vector $\vec{\mathrm{X}} \in \{\vec{\mathrm{A}}, \vec{\mathrm{B}}, \vec{\mathrm{C}}\}$ onto a segment $\mathrm{XY} \in \{\mathrm{AB}, \mathrm{AC}, \mathrm{BC}\}$ defined as:

$$\mathrm{Pr}_{\vec{\mathrm{X}}}\mathrm{XY} \cdot \tilde{v}_\mathrm{X} = (|\mathrm{XY}| \cos\theta_{\vec{\mathrm{X}},\mathrm{XY}}) \frac{\vec{\mathrm{X}}}{|\vec{\mathrm{X}}|}, \tag{6}$$

with $\theta_{\vec{\mathrm{X}},\mathrm{XY}} \in \{\theta_{\vec{\mathrm{A}},\mathrm{AC}}, \theta_{\vec{\mathrm{A}},\mathrm{AB}}, \theta_{\vec{\mathrm{B}},\mathrm{BC}}, \theta_{\vec{\mathrm{B}},\mathrm{AB}}, \theta_{\vec{\mathrm{C}},\mathrm{AC}}, \theta_{\vec{\mathrm{C}},\mathrm{BC}}\}$.

Now, the Doppler shifts of the LOS and the single bounce reflection from the vehicle "C" can be found for any symbol interval i. From the sensor-based Doppler compensation perspective, this allows the predicted channel coefficient $\tilde{h}^{\mathrm{sc}}_{i,j}$ from Eq. (3) to be represented as:

$$\tilde{h}^{\mathrm{sc}}_{i,j} = [\tilde{a}^{\mathrm{sc}}_{\mathrm{LOS}_{i,j}}, \tilde{a}^{\mathrm{sc}}_{\mathrm{C}_{i,j}}] \times \begin{bmatrix} \mathrm{e}^{\jmath 2\pi \tilde{f}_{\mathrm{D_{LOS}}_{i,j}}[i] + \tilde{\phi}_{\mathrm{LOS}}} \\ \mathrm{e}^{\jmath 2\pi \tilde{f}_{\mathrm{D_C}_{i,j}}[i] + \tilde{\phi}_{\mathrm{C}}} \end{bmatrix} + \varepsilon^{\mathrm{sc}}_{i,j}, \tag{7}$$

where $\tilde{\boldsymbol{a}} = [\tilde{a}^{\mathrm{sc}}_{i,j,\mathrm{LOS}}, \tilde{a}^{\mathrm{sc}}_{i,j,\mathrm{C}}]$ are the complex amplitudes and $\tilde{\boldsymbol{\phi}} = [\tilde{\phi}_{\mathrm{LOS}}, \tilde{\phi}_{\mathrm{C}}]$ are the predicted initial phases of the LOS component and the reflection from the vehicle "C", correspondingly; $\varepsilon^{\mathrm{sc}}_{i,j}$ represents the remaining unresolved channel components, prediction error and noise.

Based on the vector $\hat{\boldsymbol{h}}^{\mathrm{sc}}_{j}$ of L available pilot-based channel estimates at jth subcarrier and the predicted Doppler coefficients $\tilde{\boldsymbol{f}}_\mathrm{D} = [\tilde{f}_{\mathrm{D_{LOS}}}, \tilde{f}_{\mathrm{D_C}}]$, the vector of complex channel amplitudes $\tilde{\boldsymbol{a}}$ and initial phases $\tilde{\boldsymbol{\phi}}$ can be found by formulating

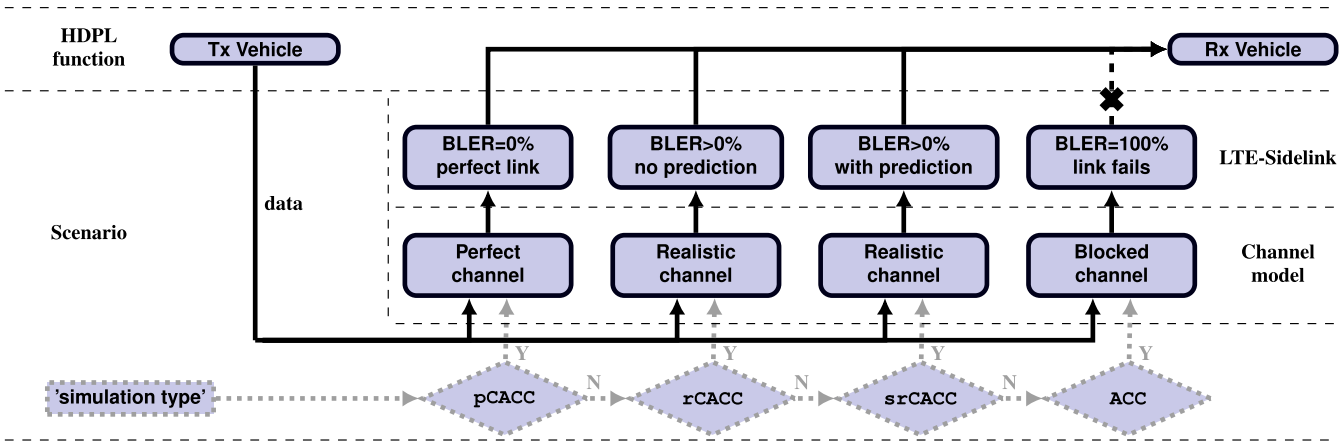

Fig. 3. Implementation flow of HDPL function affected by different qualities of link-level performance. Four cases are considered: "perfect" CACC (pCACC), BLER=0; "realistic" CACC with generic LTE-Sidelink configuration (rCACC), BLER≥0; "realistic" CACC with sensor-based Doppler compensation (srCACC), BLER≥0; "link fails" (ACC), BLER=1. Dashed gray links represent the control plane that activates the appropriate channel model.

the non-linear least square problem [27]:

$$\min_{\tilde{\boldsymbol{a}},\tilde{\boldsymbol{\phi}}} \|\tilde{\boldsymbol{h}}_j^{\mathrm{sc}} - \hat{\boldsymbol{h}}_j^{\mathrm{sc}}\|^2 = \min_{\tilde{\boldsymbol{a}},\tilde{\boldsymbol{\phi}}} \sum_{l=1}^{L} (\tilde{h}_{l,j}^{\mathrm{sc}} - \hat{h}_{l,j}^{\mathrm{sc}})^2. \tag{8}$$

Finally, based on $\tilde{\boldsymbol{a}}$, $\tilde{\boldsymbol{\phi}}$, and $\tilde{\boldsymbol{f}}_{\mathrm{D}}$, the sensor-based predicted channel coefficients can be found from Eq. (7) and the Doppler-dependent interpolation error $d(D, f_{\mathrm{D}})$, which arises from extrapolation of the estimated channel, is minimized to the level of the Doppler-independent error $\varepsilon_{i,j}^{\mathrm{sc}}$.

III. Scenario Implementation

This section describes the implementation details of the scenario of interest: HDPL affected by highly dynamic scatterers. First, the implementation of HDPL control algorithms with the vehicle and noise models is presented, then the applied channel model with highly dynamic reflecting objects is introduced. Fig. 3 illustrates the implementation flow for the HDPL function between two communicating partners with different channel and link-level configurations of interest. The implementation includes the model of the HDPL platoon function which is coupled with LTE-sidelink communications model. Furthermore, the wireless transmission is conducted over different types of communication channels, *viz.* perfect communication (pCACC), realistic channel with generic linear interpolation of the channel estimates at the receiver (rCACC), realistic channel with sensor-based Doppler compensation at the receiver (srCACC), and the worst-case scenario where communication fails completely (ACC) associated with the corresponding block error rate (BLER).

A. HDPL Control Algorithms

We develop here the algorithms that govern the motion of the HDPL vehicles. The leading vehicle is controlled by a simple proportional controller while the following vehicles apply CACC.

1) Proportional Controller: Let $v_{\mathrm{g},t}$ be the current target velocity, $v_{0,t-1}$ the velocity of the leading vehicle at time $t-1$ and k_{v} the proportional gain. The resulting acceleration command a_{c} is obtained by applying the following control law:

$$a_{\mathrm{c}} = k_{\mathrm{v}} \cdot (v_{\mathrm{g},t} - v_{0,t-1}). \tag{9}$$

2) CACC: The following CACC law is largely inspired by [2]. Let k_{v}, k_{d}, k_{p} and k_{a} be control gains. Let $x_{i,t-1}$ and $v_{i,t-1}$ be the position and velocity, respectively, of the controlled vehicle i at time $t-1$. Let $x_{i-1,t-1}^{\mathrm{s}}$ and $v_{i-1,t-1}^{\mathrm{s}}$ be the sensed position and velocity of the leading vehicle at time $t-1$ and $a_{i-1,t-1}^{\mathrm{r}}$ the received acceleration of the leading vehicle, received at $t-1$. $v_{\max}$ is the design maximal velocity, $D_{\min}$ is the minimal distance between the vehicles and T_{g} is the target IVD in seconds. As a result, $D_{\min}$ and T_{g} represent the fixed and variable components of the IVD, respectively. We can then compute the velocity components of the acceleration command, a_{v} and a_{p}. The former aims for the maximal velocity, the latter for the velocity of the previous vehicle:

$$a_{\mathrm{v}} = k_{\mathrm{v}} \cdot (v_{\max} - v_{i,t-1}), \tag{10}$$

$$a_{\mathrm{p}} = k_{\mathrm{p}} \cdot (v_{i-1,t-1}^{\mathrm{s}} - v_{i,t-1}). \tag{11}$$

The distance component, a_{d}, is given by:

$$a_{\mathrm{d}} = k_{\mathrm{d}} \cdot \left[\left(x_{i-1,t-1}^{\mathrm{s}} - x_{i,t-1} \right) - \left(D_{\min} + T_{\mathrm{g}} v_{i,t-1} \right) \right]. \tag{12}$$

The acceleration component, a_{a}, which is specific to CACC whereas the previous component were also common with ACC, is given by:

$$a_{\mathrm{a}} = k_{\mathrm{a}} a_{i-1,t-1}^{\mathrm{r}}. \tag{13}$$

Finally, the acceleration command, a_{c}, is obtained as following:

$$a_{\mathrm{c}} = \min(a_{\mathrm{v}}, a_{\mathrm{d}} + a_{\mathrm{a}} + a_{\mathrm{p}}). \tag{14}$$

This way, the following vehicle benefits from both the information received by its sensors and the data received by radio communication.

B. Vehicle Model

In order to transform the acceleration command, a_{c}, in velocity and position, we use simple numerical integration. To improve the level of realism, we add boundaries to the jerk, the acceleration and velocity. To simplify notations, in this section, we omit to mention the vehicle to which the values refer and the origin of the information, without loss of generality. The application of the control is then conducted as follows. We first apply the acceleration constraint to the acceleration command:

$$a'_{\mathrm{c}} = \max\left(\min\left(a_{\mathrm{c}}, a_{\max}\right), b_{\max}\right), \tag{15}$$

The velocity, v_t, is obtained by using the discrete numerical differentiation relationship:

$$v_t = v_{t-1} + a'_{\mathrm{c}}\Delta t, \tag{16}$$

where Δt is the sampling time. The velocity constraints are then applied:

$$v'_t = \max\left(\min\left(v_t, v_{\max}\right), v_{\min}\right). \tag{17}$$

We then derive toward the jerk in order to apply the constraints on the dynamics components.

$$a''_{\mathrm{c}} = \max\left(\min\left(\frac{v'_t - v_{t-1}}{\Delta t}, a_{\max}\right), b_{\max}\right), \tag{18}$$

$$j = \max\left(\min\left(\frac{a''_{\mathrm{c}} - a_{t-1}}{\Delta t}, j_{\max}\right), -j_{\max}\right). \tag{19}$$

Finally, we integrate back to the position in order to have all final values:

$$a_{\mathrm{c,f}} = a_{t-1} + j\,\Delta t, \tag{20}$$

$$v_{t,\mathrm{f}} = v_{t-1} + a_{\mathrm{c,f}}\Delta t, \tag{21}$$

$$x_{t,\mathrm{f}} = x_{t-1} + v_{t,\mathrm{f}}\Delta t. \tag{22}$$

This way, all constraints are satisfied and we obtain a certain level of realism in the resulting motion.

C. Sensor Noise Within HDPL

We apply Gaussian noise to all measured data. For instance, in Eq. (9), we draw one value from $\mathcal{N}(v_{0,t-1}, \sigma_{\mathrm{p}})$. σ_{p} is the standard deviation of the proprioceptive sensors, which measure ego acceleration, velocity and position. Similarly, σ_{e} is the standard deviation of the exteroceptive sensors measuring the velocity and distance of the previous vehicle. Note that the received acceleration is affected by the proprioceptive noise, as it was measured as ego acceleration before being sent.

D. V2V Channel Model

To obtain representative results while being able to take into account the impact of dynamic road objects, we employ the compromise between deterministic [28] and stochastic [29] channel modeling. Inspired by [30] and [31] we modify the widely used Spatial Channel Model (SCM) [29] by adding deterministic parameters for select road objects of interest and modifying communications parameters such as antenna heights to represent direct communication in the non-stationary vehicular environment. Similarly to [29], the considered model assumes $N = 20$ subpaths for each scattering cluster regardless of its nature.

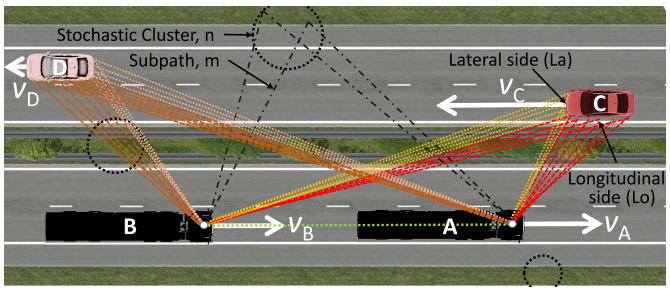

Fig. 4. The illustrative representation of the applied channel model which consists of multiple scattering clusters with stochastic properties for diffuse reflections and two deterministic objects each with two clusters of strong single bounce reflections (lateral and longitudinal sides from the oncoming vehicles).

As a result, some scatterers in the modified channel model have pre-defined properties of vehicles, traffic signs or buildings, whereas others are characterized by statistical distributions. Fig. 4 illustrates the relation between the stochastic and deterministic parameters in the applied model. The implementation details of the deterministic part are presented below.

1) Modeling Single-Bounce Deterministic Reflections: Let us assume a road object which is characterized by the strong reflectivity and is located on or in the vicinity of the road. It can be described as a regular three-dimensional solid object bounded by six rectangular sides, each of which consists of $N = 20$ subcomponents.

For the given assumptions, the amount of reflected power, P_{rf}, impinging at the receiver antenna as a single bounce reflection from a road scatterer can be described by approximation of the reflected signal components from sides of all deterministic objects visible to both communicating vehicles simultaneously. As illustrated in Fig. 1 with details highlighted in Fig. 4, the reflection caused by each deterministic road object in our model may consist of one or two reflecting areas (denoted as La and Lo in Fig. 4) depending on their relative position with respect to the communicating vehicles. If the given reflecting side of the object is located in front or behind both communicating antennas, two clusters of deterministic reflections will be impinging at the receiver, otherwise only the longitudinal side (Lo) of the given deterministic object will contribute to deterministic part of the channel.

As it is known from the two-way radar equation [10], the reflected signal power depends on the ability of the scatterer to reflect the incident energy. To incorporate such dependency, we consider a simplistic model with each side of the deterministic object being an isotropic flat rectangular plate. Then, we calculate the principal[1] bistatic radar cross-section for each $n \in N$th subcomponent of $m \in M$th

[1]Due to similar heights of the scattering object, transmitting and receiving antennas, the azimuthal angle ϕ of the incident and scattered waveform is approximated as $\phi \approx \pi/2$.

deterministic side, following the model from [32, p 591]:

$$\sigma_{n,m} = 4\pi \left(\frac{ab}{\lambda}\right)^2 \cos^2\theta_s \left(\text{sinc}\left(\frac{kb}{2}(\sin\theta_s - \sin\theta_i)\right)\right)^2, \tag{23}$$

where a, b are the dimensions of the mth subcomponent, $k = 2\pi/\lambda$, and θ_i, θ_s are the angles of the incident and reflected waves for the mth subcomponent on the horizontal plane.

2) Impact of Antenna Placement on the Power of Reflected Component: In this paper, we consider a Single Input Single Output (SISO) setup and select a rooftop placement for both transmitter and receiver antennas, as illustrated in Fig. 4. Then, via simple geometric modeling, we measure a fraction of the direct link between the antenna and an obstacle which crosses the vehicle body to estimate the actual signal attenuation level due to vehicle obstruction:

$$\gamma_\Delta(t) = \gamma_{\max} d_a(t)/d_{\max}, \tag{24}$$

where $\gamma_{\max} = \{4, 10\}$ dB [11] is the maximum attenuation level caused by the transmitting or receiving vehicle itself for light vehicle and truck, respectively; $d_{\max} = \{4.1, 16.1\}$m is the maximum and $d_a(t)$ is the actual length of the link to the scatterer which overlays the transmitting or receiving vehicle for light vehicle and truck, respectively.

The reflected signal from the vehicle located in front of the platoon is therefore stronger, whereas the reflected signal from the vehicle which just passed the platoon will have a lower reflected signal strength.

3) Received Power: The LOS channel gain is calculated according to [9]. The power reflected from the scattering object is obtained via the radar equation with the presence of ground reflection [10]:

$$P_r = \frac{P_t \lambda^2 \sigma_{n,m}}{(4\pi)^3 d_{t,r\to s}} \left(1 + \rho^2 + 2\rho\cos\left(\frac{2\pi h_{t,r} h_s}{\lambda d_{t,r\to s}}\right)\right), \tag{25}$$

where P_t is the transmitted power; λ is the signal wavelength; $d_{t,r\to s}$ is the distance from transmitter or receiver antenna to the scattering object; ρ is the reflection coefficient; $h_{t,r}$ is the height of the transmitter/receiver antenna; and h_s is the height of the geometrical center of lateral and longitudinal planes of the reflecting object.

The power of each stochastic component is calculated as in the original SCM model [29] based on the Rician K-factor, which is a ratio between the power received from the LOS and from all other stochastic reflected components. At each simulation run, a realization for the K-factor is chosen according to the selected setup and scenario. This value is drawn from the distribution provided by the extensive measurements campaigns results from [33].

4) Propagation Delay, Doppler and the Phase Shift: The signal propagation delay $\tau_{n,m}$ for the nth subcomponent of mth side is calculated using the total travel distance from the transmitter to the scatterer $d_{n,m}^{t\to s}$ and from the scatterer to the receiver $d_{n,m}^{r\to s}$:

$$\tau_{n,m} = (d_{n,m}^{t\to s} + d_{n,m}^{r\to s})/c; \tag{26}$$

The distribution of each ray parameter in specular components is now deterministic and depends on the horizontal and vertical dimensions of the considered reflecting surfaces. Finally, based on the relative location, the spread of received delays, phases, angles of departure and arrivals and the resulting Doppler shifts can be determined for each deterministic scattering object's nth subcomponent at mth side.

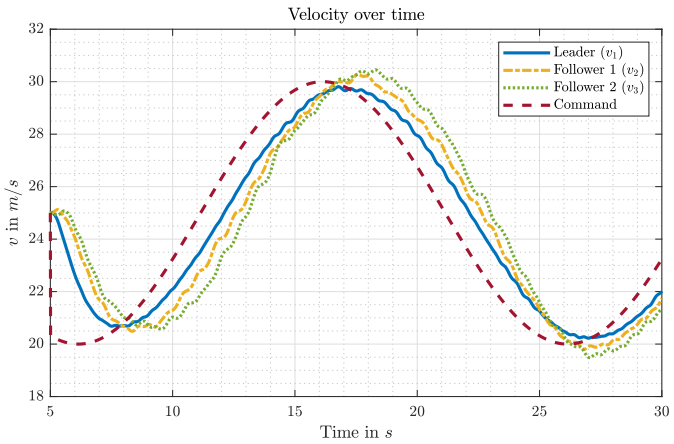

Fig. 5. Vehicle velocities with a sinusoidal command (yellow) affected by sensor noise and realistic channel.

Once the properties of deterministic scatterer with specular reflection are defined, they are added to the channel model previously described. Now all deterministic scattering components, represented as clusters of 20 sub-components, are in-line with the base SCM-model and match the overall simulation environment.

IV. Simulation Setup and Results

In this section, we first define the scenarios of interest, we then evaluate the general impact of reflecting components on the performance of HDPL. Finally, we investigate the potential for performance improvement when vehicle sensor-based link quality prediction is applied.

A. Scenarios of Interest

As mentioned in Section II-A, a plethora of possible combinations exists for the HDPL scenario: type of vehicles in the platoon, target IVD, number of lanes on the road as well as position, dimensions and reflecting properties of the scatterers. We limit our analysis on the most challenging and at the same time representative scenario, that is a three-vehicle HDPL with oncoming traffic equally spaced by 45 m on the opposite lane. We consider both a three-car and a three-truck HDPL with cars serving as oncoming vehicles in both cases. As the maximal added value of CACC over ACC is reached when acceleration is varying, we choose an artificial scenario in which the leading vehicle is given a sinusoidal command, following the setup described in [34]:

$$c(t) = v_g + 5 \cdot \sin(0.1\pi t + \psi). \tag{27}$$

This way, the effect of the perturbation introduced by the oncoming traffic on the platoon performance is emphasized. Fig. 5 illustrates the sinusoidal command (dashed maroon) and the resulting velocities of the three vehicles.

TABLE I
SIMULATION SETUP

Notation	Name	Value	Unit
Link-level parameter setup			
	Antenna config.	SISO	
$h_{\mathrm{t,r}}$	Tx and Rx ant. heights	[4, 4]	m
	Channel model used	Mod. SCM [29]	
	Num. of scenario realizations	20	
	Num. of chan. ray clusters	6	
	Num. of rays in cluster	20	
f_{c}	Carrier Frequency	5.9	GHz
	Bandwidth	1.4	MHz
	Access technique	SC-FDMA	
	Type of chan. estim.	LS [36]	
$\frac{E_{\mathrm{b}}}{N_0}$	Energy per bit to noise ratio	30	dB
$h_{\mathrm{A,B,C,D}}$	height of vehicles A, B, C, D	$[4, 4, 1.5, 1.5]$	m
$l_{\mathrm{A,B,C,D}}$	length of vehicles A, B, C, D	$[16, 16, 4.5, 4.5]$	m
$w_{\mathrm{A,B,C,D}}$	width of vehicles A, B, C, D	$[2.5, 2.5, 1.8, 1.8]$	m
$v_{\mathrm{A,B,C,D}}$	velocity of vehicles A, B, C, D	$[25, 25, 35, 35]$	m/s
Setup for HDPL model			
j	Jerk		$\mathrm{m/s^3}$
a	Acceleration		$\mathrm{m/s^2}$
v	Velocity		m/s
x	Position		m
$j_{\max}$	Maximum absolute jerk	10	$\mathrm{m/s^3}$
$a_{\max}$	Maximum acceleration	3	$\mathrm{m/s^2}$
$b_{\max}$	Maximum decceleration	-2	$\mathrm{m/s^2}$
$v_{\max}$	Maximum velocity	40	m/s
$v_{\min}$	Minimum velocity	0	m/s
$D_{\min}$	Minimum distance	0.5	m
T_{g}	Target IVD	0.2	s
v_{g}	Target speed	25	m/s
σ_{p}	Std. proprioceptive sensors	0.01	
σ_{e}	Std. exteroceptive sensors	0.04	
Δt	Time increment	10	ms
	Experiments duration	30	s
T	Number of timesteps	3000	
τ	Message period	50	ms
N_{v}	Number of vehicles	3	
$[k_{\mathrm{v}}, k_{\mathrm{p}}]$	Control parameter	[0.3, 1.1]	1/s
k_{a}	Control parameter	0.6	
k_{d}	Control parameter	0.4	$1/\mathrm{s^2}$

B. Simulation Setup

Selected combinations allow us to characterize the **generalized link-level performance** in HDPL. For our simulation setup, we use the Matlab-based V2V link-level simulation environment originally introduced at [12] and extended, as described in Sec. III-C, to reflect the impact of dynamic deterministic reflections. This simulator uses as a basis the Vienna LTE-A uplink simulator [35], but was modified to reflect key properties of direct link V2V environment, namely dual mobility, low antenna heights, distance- and environment-dependent pathloss function, six clusters of dynamic diffuse scatterers, an arbitrary number of deterministic reflecting components, *etc*. The details of the link-level parameter setup are provided in Table I. The K-factor for stochastic components is set to 10 dB, according to [33]. The communication system operates in the 5.9 GHz band.

Besides the channel model implementation, the sensor-based channel prediction originally presented in [12] and described in Sec. II-C was also incorporated into the simulator.

The simulation of HDPL functionality was then added on top of each link level communication step as described in Sec. III. The HDPL parameters used in the simulation setup are also summarized in Tab. I. In the simulated setup the leading vehicle is using the P-controller defined by Eq. (9) with $v_{\mathrm{g},t} = c(t)$ as described in Eq. (27) and Sec. IV-A. The second and third vehicles are controlled by Eqs. (10) to (14). Given the parameters provided in Tab. I, these two vehicles are targeting an IVD of 5.5 m when driving at 25 m s^{-1}. Once the target accelerations are computed by the respective controllers, the position, speed, acceleration and jerk of the vehicles are updated using Eqs. (15) and (22).

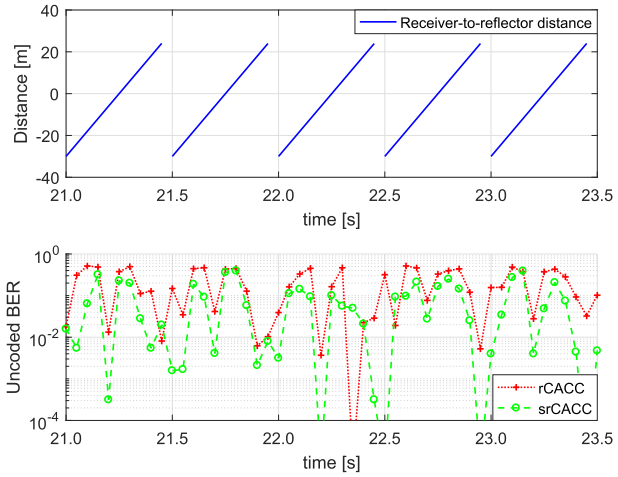

Fig. 6. An example of the HDPL performance on the highway affected by the strong reflection from the periodically oncoming vehicle. *Upper sub-figure*: the distance between the passing-by vehicle and the receiver. *Lower sub-figure*: the link-level performance for the generic communication (`rCACC`) and with sensor-based Doppler compensation (`srCACC`).

Fig. 6 illustrates an exemplary link-level performance of the developed model where cars, which serve as strong reflecting objects, pass by the HDPL. It shows how the uncoded bit error rates (uBERs) performance depends on the receiver to reflector distance. The uBER increases drastically with values reaching 0.5 for the uncompensated setup at two regions for each new vehicle passing, corresponding to the passage in front of the transmitter and behind the receiver. These regions are the most challenging for the inter-vehicle communications and are also related to the regions highlighted in Fig. 2. The uBER reported for our sensor-based solution is significantly lower for these challenging regions in most cases, staying under 0.1. Occurrences where the performances are similar, such as at times 21.75 s and 23.20 s, resulting from unresolvable stochastic components.

C. HDPL Functional Performance

In order to translate the link-level error-rate performance into the actual **HDPL functional performance** the HDPL shall be analyzed as a set of simple functional states within which the vehicle driving action remains unchanged: platoon normal driving, emergency acceleration or breaking, collision minimization, *etc.* As described in Sec. IV-A and shown in Fig. 5, out of all possible driving actions, in this work, we analyze a special case where the leading vehicle is following a sinusoidal command.

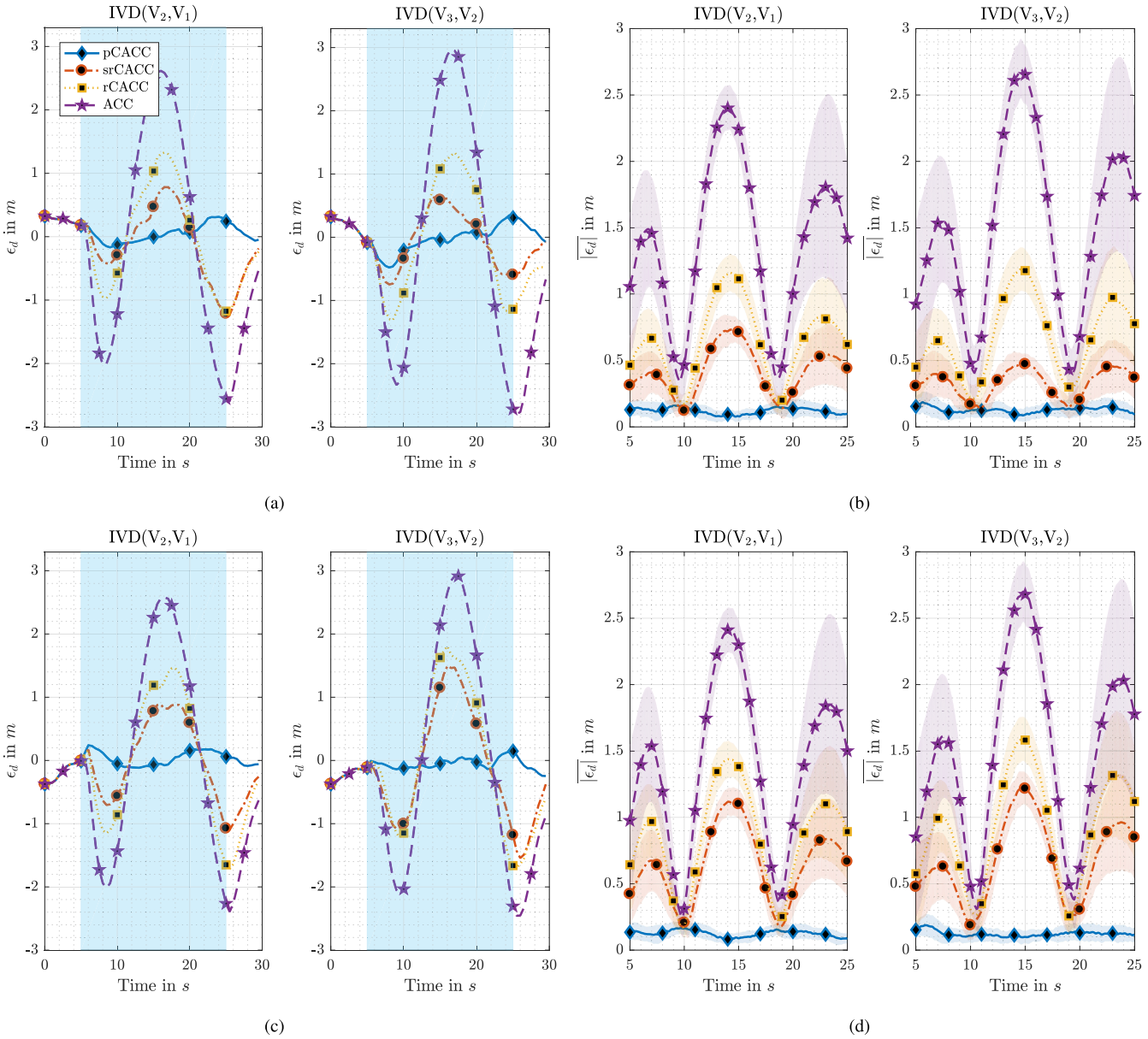

Fig. 7. Simulation results for the cars (a, b) and trucks (c, d) HDPL affected by the strong reflection component from the passing-by vehicles: Deviation from the target IVD, (a, c) for one run and (b, d) absolute average over 20 runs, after phase shift alignment. `pCACC` is denoted in solid blue, `srCACC` in dash-dotted red, `rCACC` in dotted yellow and `ACC` in dashed purple. The blue area shows the period of time in which the communication models differ. The light areas around the average curves represent the 95% confidence intervals.

D. Results

In order to compare the perturbation introduced by the incoming traffic, we perform the simulation of HDPL with three different qualities of the communication link: (1) perfect communications conditions, denoted as `pCACC`, (2) communication link affected by the presence of the realistic strong reflections from the oncoming vehicles, `rCACC`, (3) communication link fails completely and the HDPL relies on the `ACC` functionality only. In addition to `rCACC`, the sensor-based predictive Doppler compensation is applied for the scenario with realistic impact of strong reflections from the oncoming vehicles, denoted as `srCACC`. For each communication model, the vehicle simulation uses the same seed for the pseudo-random number generator, allowing us to precisely compare the impact of the communication model. The simulation starts with a 5 s stabilization period, in which the platoon uses `pCACC`. Similarly and for the same purpose, this model is used after time 25 s.

We analyze the performance of the HDPL by studying the IVD error ϵ_d, computed as following:

$$\epsilon_d(t) = \mathrm{IVD}(\mathrm{V}_i, \mathrm{V}_j)(t) - d_\mathrm{g}(t) \tag{28}$$

$$= |x_i(t) - \ell_i - x_j(t)| - (D_\mathrm{min} + c(t) \cdot T_\mathrm{g}), \tag{29}$$

where d_g is the target distance, varying between 4.5 and 6.5 m due to the component $c(t)$ defined in Eq. (27) and ℓ_i is the length of the vehicle i. Fig. 7 shows results for the different communication models using this metric. One realization of a three-car HDPL is presented in Fig. 7a. In order to reduce

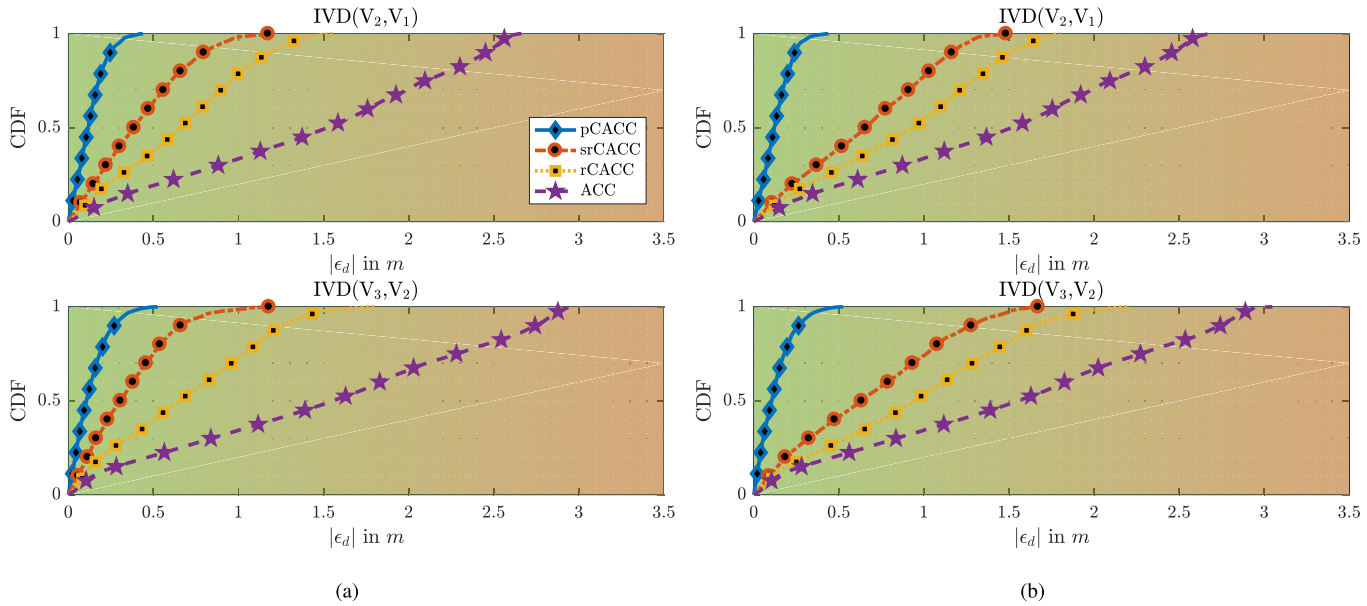

Fig. 8. Distribution of the IVD error in the cars (a) and trucks (b) scenarios. pCACC is denoted in solid blue, srCACC in dash-dotted red, rCACC in dotted yellow and ACC in dashed purple.

the impact of the sine command phase ψ on the analysis, we repeat the experiment 20 times and draw the phase value from a uniform distribution. Fig. 7b shows the average absolute deviation over all runs as a function of time, after phase realignment and focused on the period of time in which the communication models differ.

The sine shaped error observed on the single run representation (Fig. 7a) shows the effect of the perturbation on the system. With pCACC, the error is almost completely mitigated, the non-zero error is only caused by sensors imperfections introduced by the model in Sec. III-C. With the completely blocked wireless link the application relies only on its sensors and therefore performs an ACC, where the error reaches its maximum between 2.5 and 3 m. The curves of pCACC and ACC delimit the operating area of the realistic communication system. In the presence of strong scattering objects, the rCACC performs better than a completely blocked channel but the maximal error is still distributed around 1 m, thus approximately 20% of the target IVD. When using our sensor-based Doppler shift compensation algorithm, this maximal error is almost halved. These trends are holding when averaged over the multiple runs (Fig. 7b). The slightly larger confidence interval—represented by the light areas—in the 5 s–10 s and 20 s–25 s, are a side effect of the phase alignment. In this first set of results, the error for srCACC is generally around the half of the rCACC error, which is also around the half of the ACC error.

The preceding results were illustrating the performance of a three-car HDPL. In a second simulation setup, we investigate the case of three-truck HDPL, in which the distance between the antennas is larger (around 22 m considering a homogeneous setup with a truck length of 16.5 m [37] and a target IVD of 5.5 m) while the target distance is the same. Similarly to the previous setup, Fig. 7c represents the deviation from the target IVD for one run and Fig. 7d the absolute average of the error over 20 runs after phase alignment. The CACC and ACC errors are very similar to the car case, as we assume similar mechanical capabilities. However, the distribution of the srCACC error is closer to the rCACC error distribution. In a similar fashion, the distribution of the rCACC IVD error is closer to the ACC one, especially for the second pair of vehicles. In general, the error for the realistic communication simulations (rCACC and srCACC) is increased compared to the car case. This can be explained by the higher attenuation of the LOS component due to the trucks themselves, whereas the power of the reflected component with high Doppler shift, which can be compensated in srCACC case, remains the same as in the car HDPL. The latter observation shows that the separation of LOS from the deterministic reflection component by the means directional antennas might provide further performance improvements for srCACC algorithm.

We have three vehicles in our HDPL setup. It is interesting to study the differences between the two IVD values, especially when they reach their maximum. Indeed, string stability is an important feature of coupled control systems. Although the considered setup does not quantify this string stability, the study of the error differences between the pairs of vehicles provides insights into the capabilities of the systems. In pCACC, the difference in performance between the first two and the last two vehicles is insignificant, which is promising for the stability of our platooning system. In ACC, with a completely blocked channel, the error between the last two vehicles increases by almost 10%, showing the limit of our system when communications is not available. With realistic communications in rCACC, the error is rather stable at its maximum. When comparing the results of the prediction algorithm in srCACC for car and truck platoons, the error of two vehicle pairs does not follow the same pattern. If for trucks

the error is slightly higher in IVD(V_3, V_2), for cars the error in IVD(V_3, V_2) is smaller than IVD(V_2, V_1) at the peak and over time. Nevertheless, even for the trucks the perturbation for the last two vehicles is less pronounced compared to other communication models. Indeed, with a reduced perturbation on second pair of vehicles, the prediction can better stabilize the last vehicle, thus providing a twofold improvement.

The distribution of the error shows the general trend of the four compared systems. It is expressed in terms of cumulative distribution function and shown for cars in Fig. 8a and for trucks in Fig. 8b. The operating area of `rCACC` is spread between 0 and 1.5 m, therefore reaching 25% of the maximal target distance. The prediction manages to bring the performance of the platoon in a reasonable operating area, with errors under 1 m. The `pCACC` and `ACC` curves depict the best and worst case scenarios respectively. Moreover, the information about the distribution of the target distance error brings further insight into efficiency and comfort level of the driving maneuver. The larger the mismatch is, the higher the levels of acceleration and deceleration must be performed to reach the target distance. Besides the impact on string stability, these changes in velocity influence the fuel consumption and the overall level of driving comfort.

V. Conclusions

The obtained results show that the sensor-based communications prediction improves efficiency of HDPL control and maintenance process, namely reduces position, velocity and acceleration mismatches caused by imperfections in the communications link. Besides control and maintenance parameters, the proposed concept shows potential to make HDPL driving process more comfortable and fuel-efficient. The observed variations of IVD error levels in realistic CACC cases highlight the fact that packet error rate and the knowledge about expected quality of the V2V communication link plays an important role in improving HDPL performance.

References

[1] A. De La Fortelle *et al.*, "Network of automated vehicles: The AutoNet 2030 vision," in *Proc. ITS World Congr.*, 2014, pp. 1–10.

[2] S. E. Shladover, D. Su, and X.-Y. Lu, "Impacts of cooperative adaptive cruise control on freeway traffic flow," *Transp. Res. Rec., J. Transp. Res. Board*, vol. 2324, no. 1, pp. 63–70, 2012.

[3] A. Al Alam, A. Gattami, and K. H. Johansson, "An experimental study on the fuel reduction potential of heavy duty vehicle platooning," in *Proc. IEEE 13th Int. Conf. Intell. Transp. Syst. (ITSC)*, Sep. 2010, pp. 306–311.

[4] S. Tsugawa, S. Jeschke, and S. E. Shladover, "A review of truck platooning projects for energy savings," *IEEE Trans. Intell. Veh.*, vol. 1, no. 1, pp. 68–77, Mar. 2016.

[5] S. van de Hoef, K. H. Johansson, and D. V. Dimarogonas, "Fuel-efficient en route formation of truck platoons," *IEEE Trans. Intell. Transp. Syst.*, vol. 19, no. 1, pp. 102–112, Jan. 2018.

[6] A. Alam, B. Besselink, V. Turri, J. Mårtensson, and K. H. Johansson, "Heavy-duty vehicle platooning for sustainable freight transportation: A cooperative method to enhance safety and efficiency," *IEEE Control Syst. Mag.*, vol. 35, no. 6, pp. 34–56, Dec. 2015.

[7] M. Ochocki, V. Vukadinovic, M. Januszewski, and I. de la Iglesia, "Demo: Communication requirements of CACC for high-density platooning," in *Proc. IEEE Veh. Netw. Conf. (VNC)*, Dec. 2016, pp. 1–2.

[8] X. Cheng, L. Yang, and X. Shen, "D2D for intelligent transportation systems: A feasibility study," *IEEE Trans. Intell. Trans. Syst.*, vol. 16, no. 4, pp. 1784–1793, Jan. 2015.

[9] J. Karedal *et al.*, "Measurement-based modeling of vehicle-to-vehicle MIMO channels," in *Proc. IEEE Int. Conf. Commun. (ICC)*, Jun. 2009, pp. 1–6.

[10] L. Cheng, D. D. Stancil, and F. Bai, "A roadside scattering model for the vehicle-to-vehicle communication channel," *IEEE J. Sel. Areas Commun.*, vol. 31, no. 9, pp. 449–459, Sep. 2013.

[11] M. Boban, T. T. V. Vinhoza, M. Ferreira, J. Barros, and O. K. Tonguz, "Impact of vehicles as obstacles in vehicular ad hoc networks," *IEEE J. Sel. Areas Commun.*, vol. 29, no. 1, pp. 15–28, Jan. 2011.

[12] R. Alieiev, T. Hehn, A. Kwoczek, and T. Kürner, "Sensor-based communication prediction for dynamic Doppler-shift compensation," in *Proc. 15th Int. Conf. ITS Telecommun. (ITST)*, May 2017, pp. 1–7.

[13] R. Alieiev, T. Hehn, A. Kwoczek, and T. Kürner, "Predictive communication and its application to vehicular environments: Doppler-shift compensation," *IEEE Trans. Veh. Technol.*, vol. 67, no. 8, pp. 7380–7393, Aug. 2018.

[14] *Technical Specification Group Radio Access Network; Evolved Universal Terrestrial Radio Access (E-UTRA); Physical Layer Procedures*, document 3GPP TS 36.213 V12.6.0, Jun. 2015.

[15] M. Šimko, Q. Wang, and M. Rupp, "Optimal pilot symbol power allocation under time-variant channels," *EURASIP J. Wireless Commun. Netw.*, vol. 2012, no. 1, p. 225, 2012.

[16] R. MacLachlan and C. Mertz, "Tracking of moving objects from a moving vehicle using a scanning laser rangefinder," in *Proc. IEEE Intell. Transp. Syst. Conf.*, Toronto, ON, Canada, Sep. 2006, pp. 301–306.

[17] C. Merfels and C. Stachniss, "Pose fusion with chain pose graphs for automated driving," in in *Proc. IEEE/RSJ Int. Conf. Intell. Robots Syst. (IROS)*, Oct. 2016, pp. 3116–3123.

[18] J.-Y. Hong, E.-H. Suh, and S.-J. Kim, "Context-aware systems: A literature review and classification," *Expert Syst. Appl.*, vol. 36, no. 4, pp. 8509–8522, May 2009.

[19] R. Di Taranto, S. Muppirisetty, R. Raulefs, D. Slock, T. Svensson, and H. Wymeersch, "Location-aware communications for 5G networks: How location information can improve scalability, latency, and robustness of 5G," *IEEE Signal Process. Mag.*, vol. 31, no. 6, pp. 102–112, Nov. 2014.

[20] R. Alieiev, J. Blumenstein, R. Maršalek, T. Hehn, A. Kwoczek, and T. Kürner, "Sensor-based predictive communication for highly dynamic multi-hop vehicular networks," in *Proc. 25th Eur. Signal Process. Conf. (EUSIPCO)*, Aug./Sep. 2017, pp. 633–637.

[21] G. Jornod, R. Alieiev, A. Kwoczek, and T. Kürner, "Environment-aware communications for cooperative collision avoidance applications," in *Proc. IEEE 19th Int. Symp. World Wireless, Mobile Multimedia Netw. (WoWMoM)*, Jun. 2018, pp. 588–599.

[22] Y.-C. Pang, G.-Y. Lin, and H.-Y. Wei, "Context-aware dynamic resource allocation for cellular M2M communications," *IEEE Internet Things J.*, vol. 3, no. 3, pp. 318–326, Jun. 2016.

[23] T. Eyceoz, A. Duel-Hallen, and H. Hallen, "Deterministic channel modeling and long range prediction of fast fading mobile radio channels," *IEEE Commun. Lett.*, vol. 2, no. 9, pp. 254–256, Sep. 1998.

[24] F. Zeng, R. Zhang, X. Cheng, and L. Yang, "Channel prediction based scheduling for data dissemination in VANETs," *IEEE Commun. Lett.*, vol. 21, no. 6, pp. 1409–1412, Jun. 2017.

[25] S. Wender and K. C. J. Dietmayer, "Extending onboard sensor information by wireless communication," in *Proc. IEEE Intell. Veh. Symp.*, Jun. 2007, pp. 535–540.

[26] H. J. Günther, R. Riebl, L. Wolf, and C. Facchi, "Collective perception and decentralized congestion control in vehicular ad-hoc networks," in *Proc. IEEE Veh. Netw. Conf. (VNC)*, Dec. 2016, pp. 1–8.

[27] J. J. Moré, "The Levenberg–Marquardt algorithm: Implementation and theory," in *Numerical Analysis* (Lecture Notes in Mathematics), G. A. Watson, Ed. Berlin, Germany: Springer-Verlag, 1977, pp. 105–116.

[28] T. Abbas, J. Nuckelt, T. Kürner, T. Zemen, C. F. Mecklenbräuker, and F. Tufvesson, "Simulation and measurement-based vehicle-to-vehicle channel characterization: Accuracy and constraint analysis," *IEEE Trans. Antennas Propag.*, vol. 63, no. 7, pp. 3208–3218, Jul. 2015.

[29] D. S. Baum, J. Hansen, and J. Salo, "An interim channel model for beyond-3G systems: Extending the 3GPP spatial channel model (SCM)," in *Proc. IEEE 61st Veh. Technol. Conf.*, vol. 5, May 2005, pp. 3132–3136.

[30] C.-X. Wang, X. Cheng, and D. I. Laurenson, "Vehicle-to-vehicle channel modeling and measurements: Recent advances and future challenges," *IEEE Commun. Mag.*, vol. 47, no. 11, pp. 96–103, Nov. 2009.

[31] J. Karedal *et al.*, "A geometry-based stochastic MIMO model for vehicle-to-vehicle communications," *IEEE Trans. Wireless Commun.*, vol. 8, no. 7, pp. 3646–3657, Jul. 2009.

[32] C. A. Balanis, *Advanced Engineering Electromagnetics*, 2nd ed. Hoboken, NJ, USA: Wiley, 2012.
[33] L. Bernadó, T. Zemen, F. Tufvesson, A. F. Molisch, and C. F. Mecklenbräuker, "Time- and frequency-varying K-factor of non-stationary vehicular channels for safety-relevant scenarios," *IEEE Trans. Intell. Transp. Syst.*, vol. 16, no. 2, pp. 1007–1017, Apr. 2015.
[34] B. Liu, D. Jia, K. Lu, D. Ngoduy, J. Wang, and L. Wu, "A joint control–communication design for reliable vehicle platooning in hybrid traffic," *IEEE Trans. Veh. Technol.*, vol. 66, no. 10, pp. 9394–9409, Oct. 2017.
[35] C. Mehlführer, J. C. Ikuno, M. Šimko, S. Schwarz, M. Wrulich, and M. Rupp, "The Vienna LTE simulators—Enabling reproducibility in wireless communications research," *EURASIP J. Adv. Signal Process.*, vol. 2011, no. 1, p. 29, 2011.
[36] S. Pratschner, E. Zöchmann, and M. Rupp, "Low complexity estimation of frequency selective channels for the LTE-A uplink," *IEEE Wireless Commun. Lett.*, vol. 4, no. 6, pp. 673–676, Dec. 2015.
[37] European Parliament. (Apr. 15, 2014). *P7 TA(2014)0353 Dimensions and Weights of Road Vehicles Circulating Within the Community) no 6/53/ec*. [Online]. Available: https://eur-lex.europa.eu/legal-content/EN/TXT/?uri=CELEX:52014AP0353

Roman Alieiev received the Diploma (M.Sc.) degree in electrical engineering from the National Technical University KhPI, Kharkiv, Ukraine, in 2010, and the M.Sc. degree in communications and signal processing from the Technische Universität Ilmenau, Germany, in 2014. He is currently pursuing the Ph.D. degree in sensor-aided predictive vehicular communications with Volkswagen Group in conjunction with the Technische Universität Braunschweig, Germany.

As a graduate student, he was involved in different projects in the areas of wireless communications and signal processing with ST-Ericsson, Nuremberg, and the Fraunhofer Institute for Integrated Circuits IIS, Ilmenau, Germany. In 2014, he joined Volkswagen Group. From 2014 to 2017, he was with Volkswagen Group Research, Wolfsburg, Germany, where he was involved in several research projects in the areas of device-to-device communications for connected driving applications. He is currently with MAN Truck and Bus, where he is involved in vehicular connectivity. His research interests include signal processing and wireless communications for automotive applications.

Guillaume Jornod received the B.Sc. and M.Sc. degrees in environmental science and engineering (Ing. Env. Dipl. EPF) from the École polytechnique fédérale de Lausanne (EPFL), Switzerland, in 2012 and 2014, respectively, and the M.Sc. degree in management from University College London, U.K., in 2015. He is currently pursuing the Ph.D. degree in vehicle-to-vehicle communications technology diversity in conjunction with the Technische Universität Braunschweig, under the supervision of Dr.-Ing. T. Kürner.

From 2015 to 2017, he was with the Distributed Intelligent Systems and Algorithms Laboratory, EPFL, where he was a Research and Development Engineer with Prof. Martinoli and was involved in the distributed control algorithm integration and deployment for the FP7 project AutoNet 2030. In 2017, he joined the Cooperative systems and Communications Technologies Department, Volkswagen Group Research, Wolfsburg, Germany. His current research interests include adaptive and predictive quality of service for vehicular cooperative systems.

Thorsten Hehn received the Diploma degree in electrical engineering and the Ph.D. (Dr. Ing.) degree in digital communications from the University of Erlangen–Nuremberg, Germany, in 2004 and 2009, respectively. His Ph.D. thesis was on information theory and modern coding schemes, including turbo codes and low-density parity-check (LDPC) codes. His Ph.D. Advisors are Dr.-Ing. J. Huber (University of Erlangen–Nuremberg) and Prof. O. Milenkovic (University of Colorado at Boulder, USA).

As a graduate student, he was a Guest Researcher with the University of British Columbia at Vancouver, Canada. He worked with Dr.-Ing. R. Schober on optimized space-time delay-diversity codes for MIMO communications. This work later received the renowned honor ITG Preis from the German Engineering Association VDE. He worked on short-length codes and optimized decoding algorithms based on belief-propagation decoding. Also during this time, he was a Visiting Researcher with the University of Boulder, CO, USA, where he focused on error-floor problems during iterative decoding, including stopping sets and trappings sets. He joined Volkswagen Group in 2009. From 2012 to 2014, he was with Volkswagen Group of America, USA, where he was leading the Security Group of the OEM research consortium "CAMP." From 2015 to 2017, he was with Volkswagen Group Research, Germany, where he was involved in vehicle-related device-to-device communications. He is currently with Audi AG as a C-V2X/5G Developer. He has authored and coauthored many scientific papers, including publications in the renowned IEEE journal, IEEE TRANSACTIONS ON INFORMATION THEORY.

Andreas Kwoczek received the Diploma degree in electrical engineering from the Technical University of Braunschweig in 1987.

He was involved in 94-GHz transceivers and antennas at Rheinmetall Forschung and Germania Hochfrequenztechnik. In 1998, he joined Volkswagen Group, where he was responsible for the integration of car antennas. In 2007, he moved to Volkswagen Group Research, where he was responsible for the car-to-car communication hardware and evolving communication technologies. He participated in various national and international projects. Since 2012, he has been heading the group responsible for digital maps, positioning, and communication. Since 2014, the responsibility included future communications systems, i.e., 5G. Since 2017, he has been heading the Research Group for Cooperative Systems and Communications Technologies. His research interests are communication systems, antennas, and transceivers in the frequency range from sub-GHz to THz.

Thomas Kürner received the Dipl.-Ing. degree in electrical engineering and the Dr.-Ing. degree from the University of Karlsruhe, Germany, in 1990 and 1993, respectively. From 1990 to 1994, he was with the Institut für Höchstfrequenztechnik und Elektronik (IHE), University of Karlsruhe, where he was involved in wave propagation modeling, radio channel characterization, and radio network planning. From 1994 to 2003, he was with the Radio Network Planning Department at the headquarters of the GSM 1800 and UMTS operator E-Plus Mobilfunk GmbH & Co., KG, Düsseldorf, where he was the Manager of the Radio Network Planning Support Team, responsible for radio network planning tools, algorithms, processes, and parameters, from 1999 to 2003. Since 2003, he has been a Full University Professor of mobile radio systems with the Technische Universität Braunschweig. He is involved in indoor channel characterization and system simulations for high-speed short-range systems, including future terahertz communication system, propagation, traffic, and mobility models for automatic planning and self-organization of mobile radio networks and vehicle-to-X communications. In 2012, he was a Guest Lecturer with Dublin City University within the Telecommunications Graduate Initiative, Ireland. He has been engaged in several international bodies. He has actively contributed to the channel modeling document supporting the standardization of IEEE 802.11ad. He is a member of the Board of Directors of the European Association on Antennas and Propagation (EurAAP). He was the Chair of the IEEE 802.15.3d TG 100G, which developed the world's first wireless communications standard operating at 300 GHz. He is currently the Chair of the IEEE 802.15 TAG THz and is the EU Coordinator of the EU–Japan Project ThoR. From 2012 to 2017, he was the Founding Chair of the EurAAP WG Propagation.